Korean J. Chem. Eng., 36(7), 1172-1183 (2019)
DOI: 10.1007/s11814-019-0278-y

pISSN: 0256-1115
eISSN: 1975-7220

Fabrication of optimally configured layers of SWCNTs, gold nanoparticles, and glucose oxidase on ITO electrodes for high-power enzymatic biofuel cells

Xue Wang*, Joong Hyun Kim, Yong Bong Choi***, Hyug-Han Kim***, and Chang-Joon Kim*,†**

*Department of Chemical Engineering and RIGET, Gyeongsang National University, 501 Jinju-daero, Jinju, Gyeongnam 52828, Korea
**Medical Device Development Center, Daegu Gyeongbuk Medical Innovation Foundation, Daegue 41061, Korea
***Department of Chemistry, Dankook University, Cheonan 31116, Korea
(*Received 26 December 2018 • accepted 20 April 2019*)

Abstract−We designed an enzymatic biofuel cell (EFC) that utilizes indium tin oxide (ITO) electrodes, and sequential deposition of single-walled carbon nanotube (SWCNT) and gold nanoparticle (AuNP) layers on the electrodes to enhance their electron transfer. Cyclic voltammograms of the SWCNT-modified ITO electrodes showed higher peak currents compared to those of the bare ITO electrodes. Immobilization of glucose oxidase (GOD) on SWCNT-modified ITO electrodes increased their electron transfer resistance by a factor of ten, which could be mitigated by incorporating an AuNP layer between the GOD and SWCNT layers. The single-layer GOD generated higher current than the doubled-layer GOD, with higher specific activity. The assembled EFC featured SWCNT-modified ITO electrodes with sequential layers of immobilized AuNPs and GOD (anode), and with a single layer of immobilized bilirubin oxidase (BOD) (cathode). The cathode performance was further improved by the presence of AuNPs between the BOD and SWCNTs on cathode. The enhanced electron transfer kinetics and enzymatic activity observed for SWCNT/AuNP-modified ITO electrodes resulted in a maximum power density of 38.2±2.0 $\mu W/cm^2$ at 0.57±0.03 V of a cell voltage.

Keywords: Indium Tin Oxide Electrode, Single-walled Carbon Nanotubes, Gold Nanoparticles, Covalent Immobilization, Glucose Oxidase, Enzymatic Biofuel Cell

INTRODUCTION

Enzymatic biofuel cells (EFCs) consist of two bio-electrodes fabricated with immobilized enzymes that catalyze the oxidation of glucose at the anode, and the reduction of molecular oxygen at the cathode. Anode enzymes are one of glucose oxidase, glucose dehydrogenase, or cellobiose dehydrogenase, while bilirubin oxidase or laccase is cathode enzyme [1-4]. The concomitant oxidation and reduction reaction at the electrodes yields electrical power. Interest in miniature EFCs is increasing, because they are considered an alternative power source for human-implanted biomedical devices. However, the largest obstacles to miniaturization of EFCs have been the low power output and the instability of the immobilized enzymes. Recent advances in nanotechnology and biotechnology have steadily improved the performance of EFCs [1]. To date, many attempts have been made to fabricate the electrodes, which include reconstitution of an electrically contacted enzyme electrode [5], and direct electron transfer (DET) between the redox active sites of enzymes and the electrodes [5-9]. It has been also demonstrated that EFCs implanted in Rat could power electronic devices [10]. However, an obstacle facing DET-based EFCs is the low performance of EFCs associated with difficulty with the transfer of electrons between the redox center of the enzyme and the electrode due to a large distance [11]. To overcome this drawback, EFCs have been constructed using redox mediators for the efficient transfer of electrons. Heller et al. developed osmium-based redox polymer mediators for EFCs which are popularly used for EFCs because of their excellent water solubility, easy modification of their chemical structure, and their ability to control the potential of EFCs [12,13]. Additionally, carbon nanotubes (CNTs) or gold nanoparticles (AuNPs) used in EFCs to facilitate electron transfer have significantly contributed to these works. The CNTs and AuNPs both provide large surface area-to-volume ratios for enzyme immobilization and good electrical conductivity. In addition, while CNTs are electrochemically stable, intensive work has not been made on modifying CNTs and AuNPs as electrodes to increase the power output in EFCs. Therefore, further fabrication of electrodes using CNT-based nanostructured materials and enzyme immobilization with optimal configuration has been necessary to improve the performance of EFCs. Efforts have been made on fabrication of CNT yarn [14] or optimizing enzyme layers on CNT electrode [15] for EFCs. The formation of multilayer film of glucose oxidase and AuNPs or CNTs on the electrode was demonstrated to result in excellent bioelectric sensing response to the oxidation of glucose [16,17]. We previously reported that maximizing the loading of glucose oxidase (GOD) on the surface of multi-walled carbon nanotubes (MWCNTs) enhances the generation of electric power or sensing signal [18]. In most works, CNTs powder is compressed or attached on glassy carbon electrode. However, it is difficult to maintain stable compressed pellet form and/or uniform attachment of CNTs powder on the

†To whom correspondence should be addressed.
E-mail: cj_kim@gnu.ac.kr

electrode. Therefore, another fabrication technique is required to ensure the stable and uniform modification of electrodes with CNTs or AuNPs.

CNT-based thin films have been prepared by electrical, chemical, or physical methods [19]. The modification of indium thin oxide (ITO) electrode with CNTs has been also attempted [20]. ITO is commonly used in the production of plasma displays, gas sensors, and organic solar cells, because of its good optical transparency and conductivity [21]. These properties of ITO allow it to be used to monitor the behavior of electrode-grown cells [21,22], with no significant cytotoxicity observed. In addition to biocompatibility, (electro) chemically stable surface modifications of ITO electrodes allow the development of an immunosensor with high biofouling resistance, which is an important property of implantable devices designed for long-term operation [23]. Many metals, including aluminum and copper, are good candidates for electrodes, but most of them cannot be used for implantation because of their toxicity [24-26]. Furthermore, facile micropatterning of ITO electrodes enables the fabrication of microchip devices [27]. Despite these advantages, it is still challenging to develop ITO-based EFCs because of the intrinsic poor electron transfer of ITO [28-30].

Therefore, we developed a high-power EFC fabricated with ITO electrodes, where SWCNTs, AuNPs, and GOD are optimally configured. Electrodes were prepared through sequential deposition of single-walled carbon nanotubes (SWCNTs), AuNPs, and GOD layers on the surface of ITOs, and the characterization of the power-generating performances of electrodes with different configuration of these nanomaterials and GOD. Os-based redox polymers were used as mediators to transfer electrons between enzyme and surface of electrodes. The roles of all constituents were investigated by electrochemical impedance spectroscopy (EIS) and cyclic voltammetry (CV), which revealed that SWCNT layers improved the electron transfer performance of ITO electrodes. Although direct enzyme immobilization on deposited SWCNTs increased the electrode electron transfer barrier, the introduction of an AuNP layer between the GOD and SWCNT layers significantly decreased the electron transfer resistance, and improved the enzymatic activity. The EFC was assembled with GOD electrodes with optimal configuration as anode and bilirubin oxidase-immobilized ITO as cathode, then its performance was investigated.

MATERIALS AND METHODS

1. Chemicals

GOD from *Aspergillus niger* (59 units/mg, product No. G0050) was purchased from TCI (Tokyo, Japan). ITO glass sheet (100 Ω/sq) was purchased from U.I.D. (Sejong, Korea). Reagent grade sulfuric acid and hydrochloric acid were purchased from Junsei (Tokyo, Japan). Carboxylic acid functionalized SWCNTs were purchased from Sigma-Aldrich (MO, USA. product No. 652490). According to information from the provider and previous report [31,32], SWCNTs are produced by electric arc discharge technique with a carbonaceous content of 80-90% and 5-10% metallic (nickel) impurities. They were purified with nitric acid and left in a highly functionalized form with a carboxylic acid. The average diameter of individual SWCNT is 1.4±0.1 nm, and bundle dimensions are 4-5 nm× 0.5-1.5 μm. N-(3-dimethylaminopropyl)-N′-ethyl carbodiimide hydrochloride (EDC-HCl), N-hydroxysuccinimide (NHS), N-morholinoethane sulfonic acid (MES), sodium (meta) periodate, ethylene glycol, cysteamine, poly(ethylene glycol) diglycidyl ether (PEGDGE, Mn_{av}: ~500), horseradish peroxidase (product No. P6140), bilirubin oxidase from *Myrothecium verrucaria* (BOD, 25 unit, product No. B0390), *o*-dianisidine, urea, potassium chloride, and AuNP solution (product No. 753610) were purchased from Sigma-Aldrich. The osmium redox polymers, poly (N-vinylimidazole)-[Os(4,4′-dimethyl-2,2′-bipyridine)$_2$Cl])$^{+/2+}$ (PVI-Os-dme-bpy), poly (N-vinylimidazole)-[Os(4,4′-dimethoxy-2,2′-bipyridine)$_2$Cl])$^{+/2+}$ (PVI-Os-dmo-bpy), and poly (*N*-vinylimidazole)-[Os(4,4′-dichloro-2,2′-bipyridine)$_2$Cl]$^{+}$/$^{2+}$-*co*-acrylamide (PAA-PVI-Os-dCl-bpy) were synthesized according to previous reports [33,34]. The redox potentials of PVI-Os-dme-bpy, PVI-Os-dmo-bpy, and PAA-PVI-Os-dCl-bpy are 0.14, −0.025, and 0.36 V *vs*. Ag/AgCl [13,34-36]. All solutions were prepared in deionized (DI) water (1,834 MΩ-cm) unless otherwise mentioned.

2. Fabrication of SWCNT-modified ITO Electrodes

ITO glass slides (1.25 cm×2.75 cm) were cleaned by 5-min rinsing with piranha solution and 5-min sonication in DI water (160 HT, Soniclean Pty Ltd., Seoul, Korea), followed by drying in a stream of nitrogen gas at room temperature [37].

Prior to immobilization on ITO, SWCNTs (5 mg) were dispersed in MES buffer (5 mL, pH 6.0) with the aid of sonication for 3 h, followed by 10-min centrifugation at 1,106 ×*g* and 25 °C. The supernatant was decanted, and diluted to give an SWCNT solution with different concentrations. Subsequently, ITO was incubated overnight in the obtained SWCNT solution at room temperature with slow shaking. After being washed in DI water and dried at room temperature, the ITO was modified with SWCNTs (ITO-SWCNT) to afford good electro-conductivity [38] and good anchoring points for the covalent attachment of AuNPs and enzymes. The amount of SWCNTs adsorbed on ITO was estimated as the difference between the amounts of SWCNTs in solutions before and after incubation. To measure the concentration of SWCNTs in solution, the supernatant and pellet were separated by centrifugation from 10 mL of SWCNT dispersion (1 mg/mL), and were then transferred to weighed aluminum dishes. After drying at 80 °C for 2 h in a vacuum oven, the dried weight of supernatant or pellet was calculated by subtracting the weight of aluminum dish. This supernatant with known concentration of SWCNTs was used as standard solution for preparing the calibration curve. The concentration of SWCNTs remaining in supernatant after adsorption was determined by measuring the absorbance at 300 nm using an ultraviolet/visible (UV/Vis) spectrophotometer (UV-1601, Shimazu, Japan), based on the calibration curve as described by Attal et al. [39]. The calibration curve prepared from a SWCNTs solution with known concentration was linear up to 22 μg/mL of SWCNTs.

3. Preparation of Enzymes and AuNP Layer on ITO-SWCNT Electrodes

Before immobilization, the carbohydrate groups on the peripheral surface of GOD were oxidized to carbaldehydes, as follows. A solution of GOD (20 μM) in phosphate buffer saline (PBS; 5 mL, pH 6.8) was reacted with sodium metaperiodate ($NaIO_4$; 6 mg/mL) for 1 h at 4 °C in the dark. Subsequently, the reaction was quenched

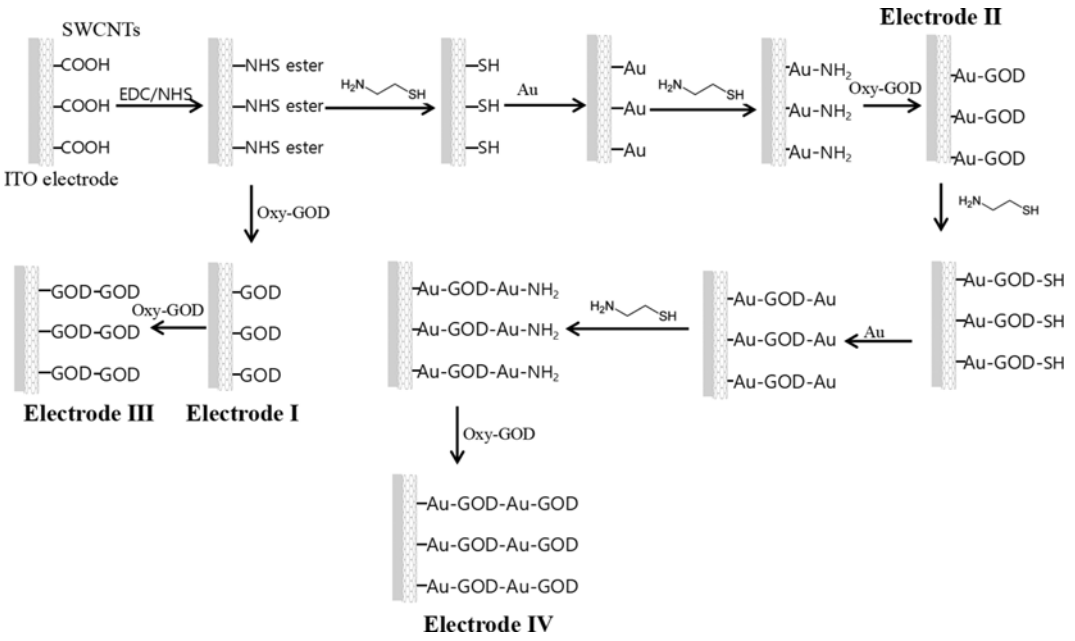

Fig. 1. Schematic illustration of the layer-by-layer immobilization of SWCNTs, AuNPs, and GOD on ITO electrodes.

with 25 mM ethylene glycol, and left at 25 °C for 30 min. The reaction solution was dialyzed (12,000-14,000 MWCO membrane) and then concentrated with ultrafiltration (30,000 MWCO membrane), following the previously documented procedure [16].

Grafting of oxidized/purified GOD (oxy-GOD) or AuNPs on SWCNTs was initiated using EDC/NHS coupling at optimized condition [18]. Briefly, ITO-SWCNT slides were immersed in MES buffer (2 mL, 100 mM, pH 6.0) containing EDC (52 mM) and NHS (430 mM), followed by shaking at 160 rpm for 3 h at 25 °C. The slides were thoroughly rinsed with the same buffer to remove unreacted residues and the urea by-product. Four types of GOD-attached ITO electrodes (electrodes I, II, III, and IV) were prepared by conjugating oxy-GOD with amine-reactive or AuNP-conjugated ITO-SWCNT slides (Fig. 1). Electrode I was fabricated by conjugating oxy-GOD with NHS ester-activated SWCNTs. The activated SWCNTs adsorbed on ITO glass were treated with MES buffer (2 mL, 100 mM, pH 6.0) containing oxy-GOD (8.7 mg/mL), followed by 3 h shaking at 160 rpm and 25 °C. Electrode II was prepared by fabricating AuNP layer and GOD layer sequentially on the activated SWCNTs on ITO glass, respectively. The AuNPs and GOD layers were assembled by attaching AuNPs on aminated SWCNTs, followed by grafting oxy-GOD on the produced AuNPs layer, using cysteamine as a cross-linker. In detail, the NHS-ester activated ITO-SWCNT glass was immersed in cysteamine solution (20 mM, 2 mL) and incubated in darkness for 2 h at 25 °C, followed by washing with DI water. The ITO-SWCNT glass bearing thiol group (-SH) was incubated for 2 h in a 2-mL AuNP solution, which was used as received with no dilution, to form Au-S bonds between AuNPs and SWCNTs on ITO. The AuNP-SWCNT-grafted ITO glass slides were reacted with cysteamine, and washed with DI water, with covalent linking of oxy-GOD aldehyde groups to cysteamine NH_2 groups performed by immersing the above slides into oxy-GOD solution for 2 h [16]. Electrode III was prepared by incubating electrode I in oxy-GOD solution, without further treatment. Electrode IV was prepared by subjecting electrode II to the above procedure of AuNP and GOD layer formation.

The BOD cathode was prepared by immobilizing BOD and PAA-PVI-Os-dCl-bpy on ITO-SWCNT electrodes through physical adsorption. A solution of BOD or BOD-AuNP mixture with 250 unit/mL of BOD activity, a stock solution of PAA-PVI-Os-dCl-bpy (10 mg/mL) and PEGDGE (10 mg/mL) were mixed in a 4 : 4 : 1 ratio (v : v : v). The obtained mixture (8 μL) was placed on the surface of the ITO-SWCNTs, followed by drying for 1 h at room temperature.

4. Surface Characterization of Electrodes and Biochemical Analyses of Immobilized GOD

Transmission electron microscopy (TEM) measurements were performed on an FEI TECNAI TF30ST at an acceleration voltage of 300 kV. A drop of SWCNT dispersion or supernatant was placed onto a carbon-coated TEM copper grid. TEM images were recorded using CCD cameras installed in this microscope. The surface morphology of bare or SWCNT-modified ITO was investigated by field emission scanning electron microscopy (FESEM) using a JEOL JSM 7610F instrument operated at an acceleration voltage of 5 kV.

The chemical composition of the GOD-attached ITO electrodes was analyzed using X-ray photoelectron spectroscopy (XPS, AXIS Ultra-delay Line Detector, Kratos, UK) at the Korea Basic Science Institute (Daejeon, Korea). Electrode analyses were also performed using Raman spectroscopy and energy dispersive X-ray (EDX) spectrometry, as described in the supplementary section.

The amount of immobilized enzyme (GOD loading) on the electrodes was indirectly estimated by measuring the concentration of flavin adenine dinucleotide (FAD) related to the amount of immobilized GOD, following a previously described procedure [18]. Briefly, GOD-modified ITO electrodes were soaked in 5 mL

of a solution containing 8 M urea and 0.05 M KCl for 2 h, and the concentration of FAD released from immobilized GOD was estimated by measuring the fluorescence of the solution (emission at 520 nm, and excitation at 375 nm; LS-50B, PerkinElmer). The calibration curve prepared using a series of standard FAD solutions was linear up to 60 nM. Alternatively, the loading of GOD was estimated by the difference between the amounts of enzyme in the GOD solution before and after coupling reaction and desorbed during washing cycle [18]. The amount of enzyme was determined by measuring the protein content of enzyme solution using a commercial kit (Thermo Scientific, Rockford, IL, USA) following the protocol supplied by the company. The GOD loading was expressed as the amount of immobilized GOD per unit area of electrodes.

The activity of free and immobilized GOD was measured from a coupled-enzyme assay using horseradish peroxidase and *o*-dianisidine. The assay solution was prepared by mixing 2.5 mL of 1 wt% *o*-dianisidine in 0.1 M potassium phosphate buffer (pH 6.0), 0.3 mL of 18 wt% glucose in DI water, and 0.1 mL of 0.2 mg/mL horseradish peroxidase. The resulting mixture was saturated with oxygen by bubbling air for 30 min, and its 2.9-mL aliquot was used to treat a solution of free GOD (0.1 mL, 0.1 mg/mL) or GOD-immobilized ITO in a spectrophotometer cuvette, with the absorbance increase at 460 nm measured at one-minute intervals using UV-vis spectrophotometer. The specific activity of GOD was calculated from the initial linear portion of the obtained curve and the known GOD content.

5. Electrochemical Analyses of Immobilized Enzyme and EFC Performance

The electrochemical cell consisted of a three-electrode system with working electrode, Pt wire (counter electrode), and Ag/AgCl in saturated KCl (reference electrode). The EIS measurements were captured in the presence of 10 mM $K_3[Fe(CN)_6]/K_4[Fe(CN)_6]$ (1 : 1) mixture as a redox probe in the frequency range 0.1-100,000 Hz at the formal potential of the system, E^o=0.23 V. The amplitude of the alternate voltage was 5 mV. The CV measurements were performed at scan rate of 10 mV/s in PBS (pH 7.0) for ITO-SWCNT or PBS (pH 7.0), supplemented with glucose (30 mM) for GOD-immobilized ITO as an electrolyte. The ITO-SWCNT or enzyme immobilized ITO electrodes were used without further modification for the EIS measurements. However, working electrodes were prepared by modifying the immobilized GOD (anode), and BOD (cathode) with osmium-containing redox mediators, according to the previously described procedure [18,40], for CV analysis or EFC test. For CV analyses of SWCNT-coated ITO or GOD-attached ITO electrodes, PVI-Os-dme-bpy was used as a common mediator. However, PVI-Os-dmo-bpy was used as an anode mediator for full-cell test because the high potential gap between anode and cathode results in high power output. A stock solution of PVI-Os-dme-bpy (10 mg/mL, for GOD electrode in CV analysis) or PVI-Os-dmo-bpy (10 mg/mL, for anode in EFC) was mixed with PEGDGE (10 mg/mL) in a 4 : 1 ratio (v : v), and the obtained mixtures (8 μL) were drop-cast on the surfaces of GOD-immobilized ITO glass slides, respectively, followed by 1 h drying at room temperature. According to the procedure, the amount of adsorbed Os-polymer was 64 μg per cm^2 of electrode surface.

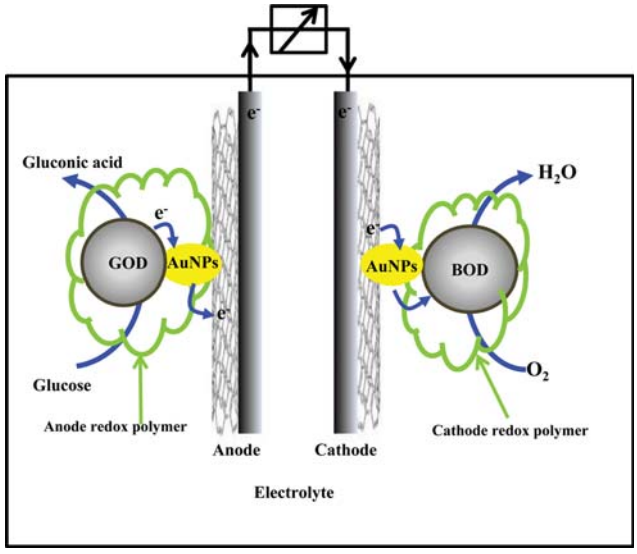

Fig. 2. Schematic diagram of the ITO-based EFC running with glucose.

Fig. 2 shows the working principle of the assembled EFC which comprised the anode and cathode. Anode and cathode were placed in 250-mL beaker, which was filled with a solution of glucose (30 mM) in PBS (150 mL, pH 7.0) saturated with oxygen. All electrochemical measurements were performed at room temperature in a Faraday cage, using an electrochemical workstation (CH Instruments, model 660d, Houston, USA) interfaced to a computer. The EFCs discharge curves were recorded at variable discharge currents.

RESULTS AND DISCUSSION

1. Preparation and Characterization of SWCNT-modified ITO Electrodes

The supernatant of SWCNT dispersion made a thin-film coating over ITO by physical adsorption in this study. It was estimated that ~60% of SWCNTs was pelleted out during the centrifugation of 1 mg/mL SWCNT dispersion, with the residual SWCNT concentration in the black-colored supernatant equal to 350 μg/mL. The TEM image shows that the most of SWCNTs in the supernatant were debundled (Fig. 3(b)), whereas entangled SWCNT bundles were observed in SWCNT dispersion before centrifugation (Fig. 3(a)). Since nanotube bundles and aggregates could be easily removed by centrifugation [41], we could obtain well dispersed SWCNTs in supernatant.

The above supernatant was diluted to give concentrations of 87, 161, and 338 μg/mL, and the resulting solutions were used to coat ITO slides with SWCNTs. After incubation, the color of the slides changed to dark gray, and the slide was darker in solution with higher concentrations. Fig. 4(a) shows that the amount of SWCNTs adsorbed on ITO (SWCNT loading) increased with increasing SWCNT concentration in solution, whereas the adsorption efficiency (~5.5%) was not influenced by the applied concentrations. Three ITO slides with different SWCNT loadings (9.3±0.1, 18.1±5.8, and 36.7±1.6 μg/cm^2) were prepared, and SWCNT coverage

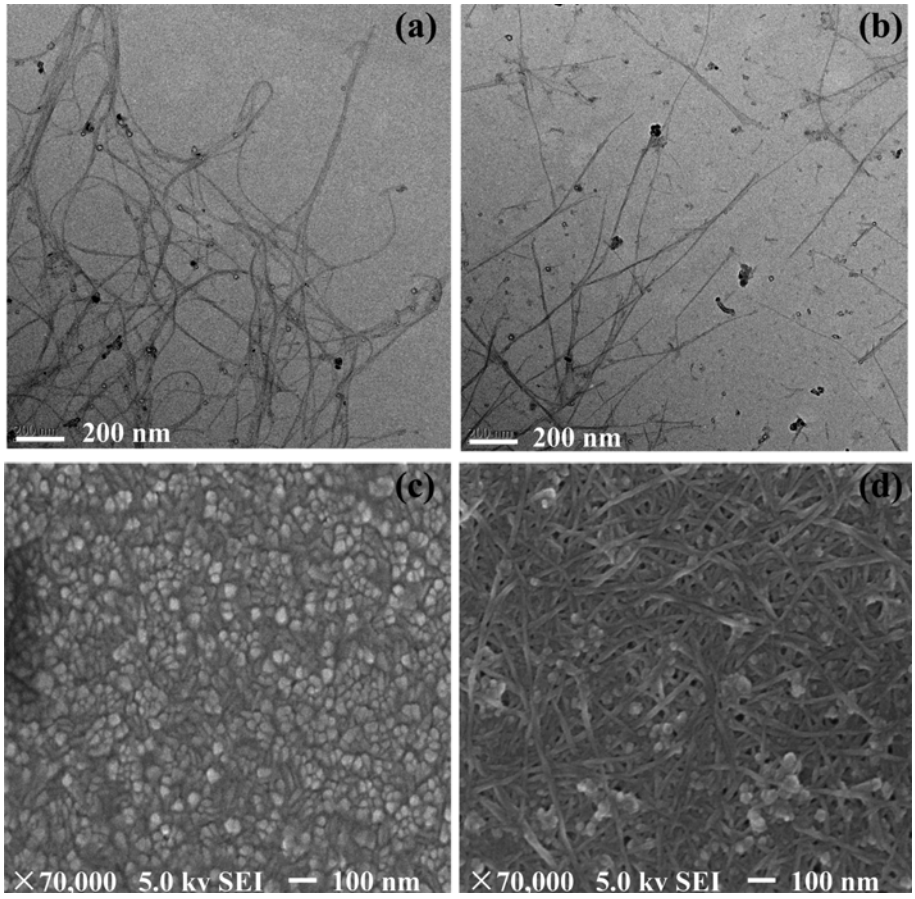

Fig. 3. TEM images of (a) SWCNT dispersion and (b) SWCNT supernatant. SEM images of (c) bare ITO and (d) SWCNT-coated ITO (37-SWCNT-ITO).

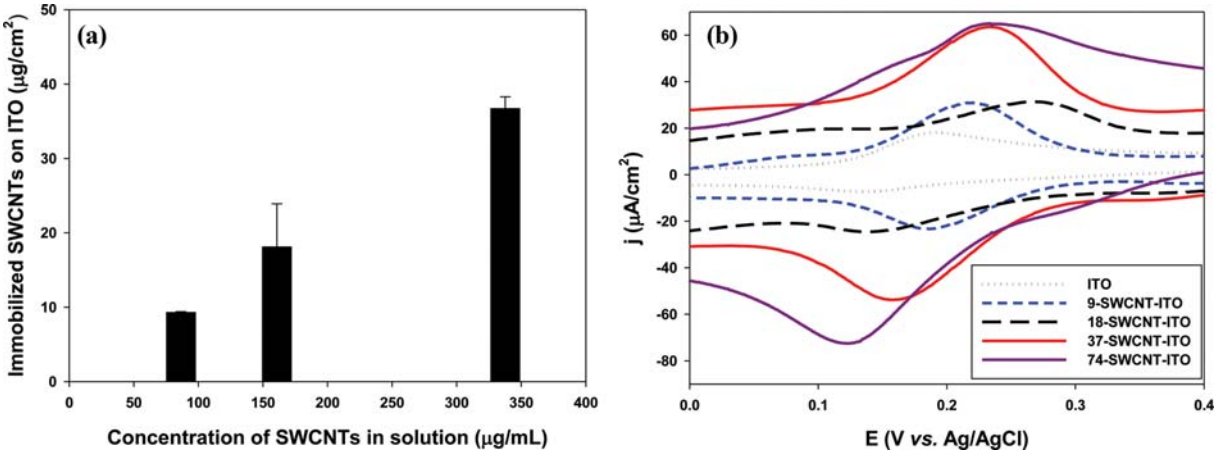

Fig. 4. Characterization of ITO electrodes with different SWCNT loadings. (a) The amount of immobilized SWCNTs onto the surface of ITO electrode in SWCNT solutions with different concentrations and (b) cyclic voltammograms for the different ITO electrodes (ITO, 9-SWCNT-ITO, 18-SWCNT-ITO, 37-SWCNT-ITO, 74-SWCNT-ITO). Electrodes were modified with redox polymer (PVI-Os-dme-bpy), and then cyclic voltammetry measurements were performed in PBS (pH 7.0) at scan rate of 10 mV/s.

was examined by Raman spectroscopy. Fig. S1 shows the characteristic Raman peaks of CNTs, such as their D (1,347 cm^{-1}), G_+ (1,592 cm^{-1}), and G_- bands (1,569 cm^{-1}), and wire-like CNT patterns in Raman mapping images, indicating the successful immobilization of SWCNTs on ITO slides [42]. The area and thickness of Raman scatterings of SWCNTs also increased in proportion to the loading amount of SWCNTs. Figs. 3(c) and (d) show the FESEM images of the surface morphology of bare ITO and ITO

with SWCNT loading of 36.7±1.6 μg/cm^2. SWCNT networks were clearly observed on SWCNT-coated ITO, whereas bare ITO exhibited aggregates of spherical particles, typical surface morphology of ITO. Together with Raman spectroscopic analysis, this evidence clearly indicated that coverage of SWCNTs on ITO could be controlled by varying the concentration of the SWCNT solution used for incubation. Furthermore, SWCNTs were adsorbed well and homogeneously layered on the ITO electrode.

SWCNT-coated ITO electrodes (ITO-SWCNTs) were characterized by CV analyses, which were performed using a mediator (PVI-Os-dme-bpy) immobilized on ITO-SWCNTs. Fig. 4(b) shows the CV curves recorded in PBS (pH 7.0) for ITO-SWCNTs modified with the above mediator, revealing oxidation and reduction peaks corresponding to the Os (II/III) transition at 0.2 V (vs. Ag/AgCl). The peak current densities (j) observed for ITO-SWCNTs were higher than that of bare ITO glass in PBS, with the maximum current density obtained at an SWCNT loading of 37 μg/cm^2 (37-SWCNT-ITO). It was considered that the large surface area of ITO-SWCNTs enhanced the electron transfer capability of the electrodes, resulting in higher electrochemical current than that observed for the bare ITO electrode. Also, increased SWCNT loadings were shown to promote the electron transfer capability of ITO-SWCNTs. Therefore, the incubation of ITO slides was repeated twice in fresh SWCNT solution (338 μg/mL), and ITO with higher SWCNT loadings (74±5.9 μg/cm^2) was obtained. However, no further increases in peak current density were observed with further increases in SWCNT loading (74±5.9 μg/cm^2). This indicates that the SWCNT coating (~37 μg/cm^2) facilitates electron transfer [43,44], but the extra thickness of the immobilized SWCNT layer may affect electron transfer by increasing the electron transport distance. According to Sone and Yagi [45], carboxylated SWCNTs are adsorbed on ITO electrode by chemical interaction between carboxyl groups and the ITO surface. They also revealed that the SWCNT layer increased the capacitance of electrode, interfacial area between electrode surface and electrolyte, thereby resulting in higher current generation.

2. Surface Characterization of GOD-immobilized Electrodes by X-ray Photoelectron Spectroscopy (XPS)

The oxy-GOD or AuNPs were covalently attached onto ITO with optimal SWCNT loading (37-SWCNT-ITO), and Fig. 1 shows the fabrication process of four different GOD-immobilized electrodes. To verify the conjugation of GOD with AuNPs or SWCNTs, we characterized the surface compositions of the layers fabricated on ITO electrodes. Fig. S2 shows the EDX analyses, in which the major peaks observed in the four electrodes were In, Sn, O, Si, Na, Mg, Al, and Cl, which are major components of the ITO electrode [46]. Strong Au peaks were observed on electrodes II and IV, while they were not observed on electrodes I and III. The data confirms the successful binding of AuNPs onto electrodes II and IV.

XPS analyses of the surfaces of electrode II were also performed in comparison with ITO-SWCNT. The wide scan spectra of ITO-SWCNT in both Figs. 5(a) and (c) show peaks located at 444.3 eV ($3d_{5/2}$) and at 451.1 eV ($3d_{3/2}$) corresponding to indium, and at 486.0 eV ($3d_{5/2}$) and 495.2 eV ($3d_{3/2}$) corresponding to tin [47]. The higher peak of O1s (532.8 eV) revealed in Fig. 5(d), along with the appearance of a stronger N1s peak on electrode II (ITO-SWCNT-Au-GOD) than ITO-SWCNT, indicates the presence of GOD on the electrode, as O and N were expected from the backbone amide and carboxylic groups of GOD, respectively [48]. Figs. 5(b) and (e) show that the C1s peaks of two electrodes could be deconvoluted into three peaks at 285.5, 286.7, and 289.4 eV, which

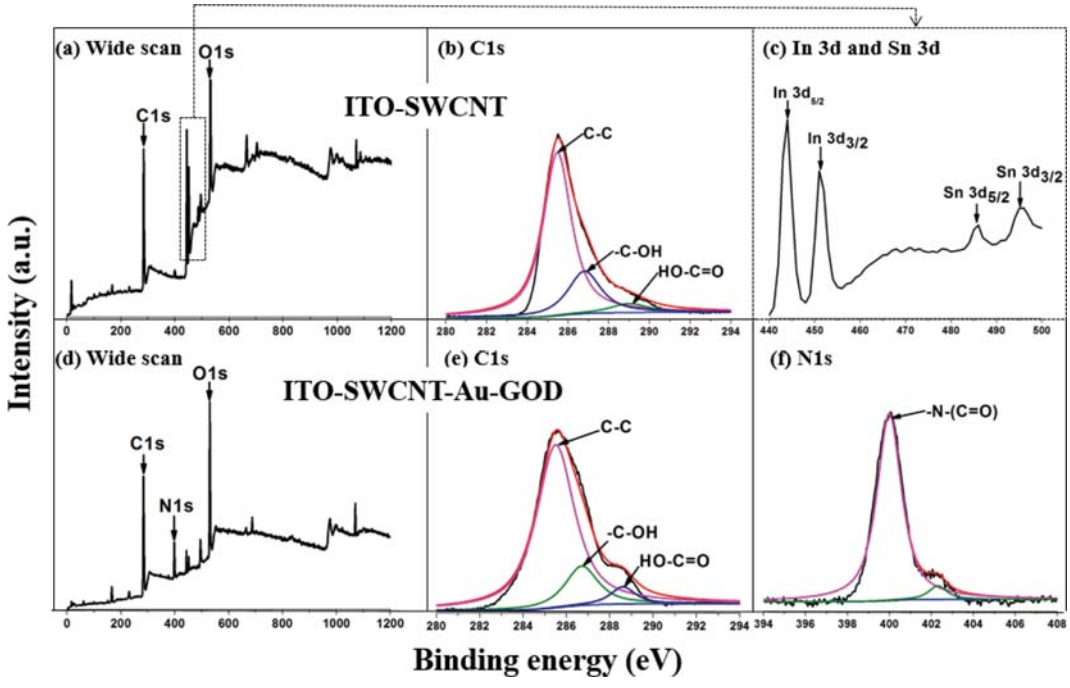

Fig. 5. XPS spectra of the ITO-SWCNT and ITO-SWCNT-Au-GOD. (a), (c) and (d) Survey spectra, and (b), (e) and (f) XPS spectra of N1s, and C1s core levels, respectively.

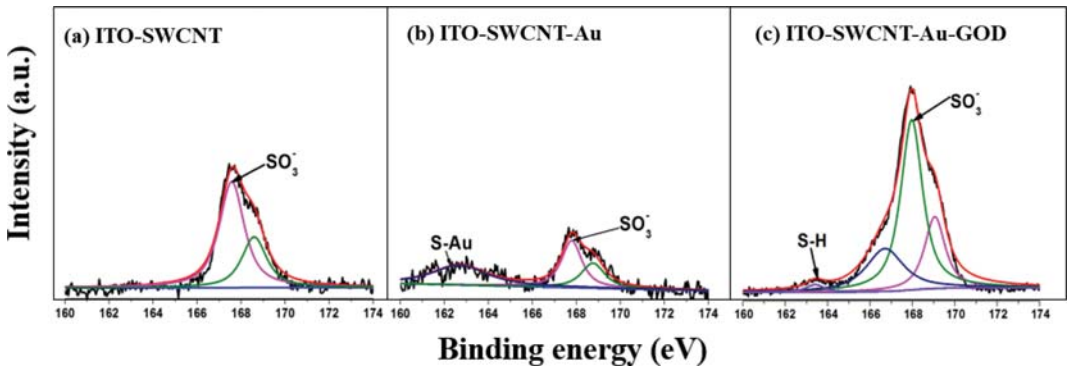

Fig. 6. XPS spectra of (a) ITO-SWCNT, (b) ITO-SWCNT-Au, and (c) ITO-SWCNT-Au-GOD showing S2p high resolution spectra.

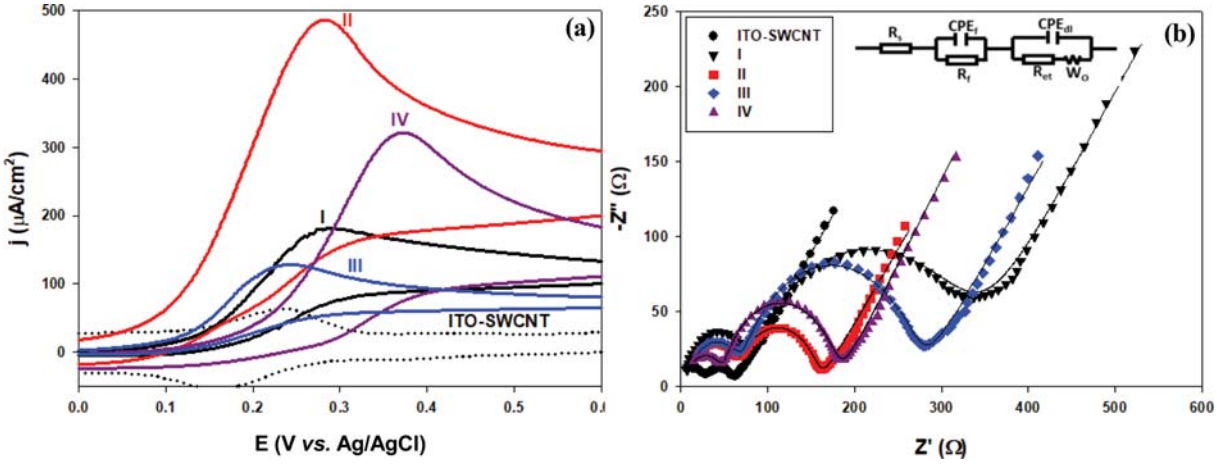

Fig. 7. Characterization of ITO-SWCNT electrodes with different configurations of immobilized AuNPs and GOD. (a) Cyclic voltammograms and (b) electrochemical impedance spectra of electrode I (ITO-SWCNT-GOD), II (ITO-SWCNT-Au-GOD), III (ITO-SWCNT-GOD-GOD) and IV (ITO-SWCNT-Au-GOD-Au-GOD). Electrodes were modified with redox polymer (PVI-Os-dme-bpy), then cyclic voltammetry measurements were performed in PBS (pH 7.0) supplemented with 30 mM of glucose at scan rate of 10 mV/s.

are assigned to C-C bonds of graphitic carbon, -C-OH, and HO-C=O, respectively, indicating the typical C1s spectra of carboxylated carbon nanotubes [49,50]. The peak of carboxyl group (HO-C=O) in electrode II dramatically increased compared to that of ITO-SWCNT, indicating the formation of covalent bonds between GOD and the SWCNTs via AuNPs [49,51]. Fig. 5(f) shows that the binding energy at 400 eV in the N1s spectra was assigned to the formation of amide bonds [51,52] on the surface of electrode II, which further confirms the covalent binding of GOD onto the electrode. Fig. 6 shows a comparison between (a) ITO-SWCNT, (b) ITO-SWCNT-Au, and (c) ITO-SWCNT-Au-GOD (electrode II) in the S2p region. The ITO-SWCNT-Au shows a peak at ~162.5 eV which is assigned to the sulfur bound to the AuNPs (S-Au) [53], whereas the peak of electrode II remained at ~163.5 eV, corresponding to the sulfur of the free thiol group (S-H) [54], which is presumably attributed to the single cysteine residue in GOD [53]. The free sulfite (SO_3^-) peak at ~168.8 eV likely originated from MES buffer components left in the sample. The results of the EDX and XPS analyses clearly demonstrate that AuNPs were bound on SWCNTs functionalized with thiol (cysteamine) via thiol-gold bonding, and that GOD was covalently attached onto the surface of AuNPs on electrode II.

3. Electrochemical Characterization of GOD-immobilized Electrodes

The electrochemical properties of GOD-immobilized electrodes were characterized by CV and EIS. In the absence of glucose, all electrodes showed small and quasi-reversible peaks, which represent the redox couple responsible for the redox reaction of the mediator, PVI-Os-dme-bpy (Fig. S3). However, upon addition of 30 mM of glucose to the PBS (pH 7.0), a sharp increase in the anodic current was observed at potential around 0.3 V (vs. Ag/AgCl) for GOD-immobilized electrodes, whereas the curve of ITO-SWCNT was not affected by the presence of glucose, as shown in Fig. 7(a). Compared with the CV curves in the absence of glucose, a cathodic current was not observed for GOD-immobilized electrodes, which was ascribed to the fast reduction of mediator in the enzymatic reaction. These sigmoidal voltammograms are characteristic of enzymatic glucose oxidation, wherein the electron transfer mediated by the osmium redox polymer is directed from the enzyme active site to the electrode. The peak current density (j) of electrode I was ~3 times higher than that of ITO-SWCNT. Table 1 summarizes the GOD loading and electrochemical properties of

Table 1. Electrochemical properties of the four electrodes with different GOD loadings or AuNPs

Electrode	Description	GOD loading ($\mu g/cm^2$)	Peak current density ($\mu A/cm^2$)	Peak current/GOD ($\mu A/\mu g$)	R_{et} (Ω)
I	ITO-SWCNT-GOD	35.3±5.8	182.6±20.7	5.2±0.4	266.1
II	ITO-SWCNT-Au-GOD	26.2±1.0	484.4±66.5	18.5±0.7	92.5
III	ITO-SWCNT-GOD-GOD	56.4±3.8	128.1±10.8	2.3±0.3	206.1
IV	ITO-SWCNT-Au-GOD-Au-GOD	35.6±2.2	320.2±59.4	9.0±2.1	131.5

the four electrodes.

Since GOD contains two FAD molecules as cofactor, we estimated immobilized GOD on the electrodes by measuring released FAD from denatured GODs. For electrode II, it was estimated that 26.2±1.0 μg of GOD was immobilized per cm^2 of electrode. For comparison, GOD loading was also estimated by measuring the difference in the protein concentration of the solution before and after coupling reaction. The GOD loading for electrode II was 31± 1.7 μg per cm^2 of electrode, which was fairly in good accordance with the value estimated by the amount of released FAD. We also demonstrated a similar result in a previous study [18]. Therefore, GOD loadings of other electrodes were estimated by measuring the amount of FAD released after denaturing the immobilized GOD.

The introduction of a AuNP layer between the GOD and SWCNT layers (in electrode II) increased the current density to 484.4±66.5 $\mu A/cm^2$, which was 2.7-times higher than that of electrode I, although the amount of GOD immobilized on electrode II (26.2±1.0 $\mu g/cm^2$) was less than that deposited on electrode I. The catalytic current of electrode III decreased even for GOD amount (56.4±3.8 $\mu g/cm^2$), exceeding that deposited on electrode I, but a 2.5-fold increase in current compared to electrode III was observed by incorporating AuNPs between the GOD layers in electrode IV. The AuNPs and GOD layers were expected to play a critical role in electron generation and transport. Therefore, to identify how the AuNPs and GOD layers affected the current, we performed additional EIS characterization of each electrode in the presence of 10 mM $Fe(CN)_6^{3-/4-}$ and the impedance spectra were fitted with the equivalent circuit inset and fitting curves are shown in Fig. 7(b) as solid lines, together with the experimental data denoted as symbols. The plots show good agreement in terms of simulated and experimental EIS. R_s denotes the solution resistance, which is the resistance between the reference and working electrodes. The first semicircle (at a high frequency) is ascribed to the resistance of the surface film (R_f) arising from the coating materials (ITO, SWCNTs, or AuNPs), and the second semicircle (at a high-medium frequency) is associated with the resistance of electron transfer (R_{et}) at the electrode/electrolyte interface. Additionally, the CPE_f and CPE_{dl}, constant phase elements are related to the capacitances of the coating material and double layer of electrode/electrolyte, respectively. The slope line in low frequencies, referred to as open Warburg impedance (W_o), results from the resistance of ion diffusion [55, 56]. As R_s and W_o represent the bulk properties of the electrolyte solution and diffusion feature of the redox probe in solution, respectively, they are not affected by chemical transformations occurring at the electrode surface. On the other hand, R_{et} (second semicircle diameter) varies by the properties depending on the dielectric and insulating properties of the electrode/electrolyte interface, and changes in R_{et} can be employed as a signal to characterize the electrode modification [16,55,56]. Therefore, the electron transfer process occurring on ITO-SWCNTs was examined by measuring their R_{et} in the presence of $Fe(CN)_6^{3-/4-}$.

Fig. 7(b) shows that significantly different spectra can be obtained depending on the configurations of the AuNPs and GOD immobilized on ITO-SWCNT electrodes. The smallest second semicircle was observed for ITO-SWCNT, indicating the lowest charge (electron) transfer resistance, whereas the direct conjugation of GOD to SWCNTs on the ITO electrodes (electrode I) resulted in a large increase of electron transfer resistance (R_{et}=266.1 Ω from Table 1). Notably, the diameter of the second semicircle was decreased by introducing AuNPs between GOD and SWCNTs, indicating a dramatic decrease of electron transfer resistance. The result indicates that GOD acts as a barrier to the interfacial electron transfer, whereas AuNPs are excellent electron transfer promoter. Several reports also showed that the electron transfer resistance of SWCNT-modified electrodes could be further decreased by the immobilization of AuNPs on their surface [55,57], which was attributed to the excellent conductivity of these metallic nanoparticles.

In addition to being influenced by conductivity, the electron transfer kinetics is also affected by the charge of materials on electrode interfaces. Electrostatic repulsion between negatively charged molecules and $Fe(CN)_6^{3-/4-}$ results in increased electron transfer resistance because the repulsion of the same charge of the molecules hinders the interfacial electron transfer of the redox probes. In addition, insulating biomolecules, such as enzymes, can block electron transfer on the electrodes, which results in increased electron transfer resistance. Since GOD is negatively charged at neutral pH [58], the electrostatic repulsion and poor conductivity of the insulating layer were expected to increase the interfacial electron transfer resistance. In contrast, positively charged cysteamine-modified AuNPs were expected to weaken the electrostatic repulsion. Consequently, the electron transfer was accelerated by the presence of AuNPs between GOD and the SWCNTs on ITO electrodes, due to the electrostatic attraction as well as good conductivity of these metallic nanoparticles. Immobilization of additional GOD and AuNPs on electrode II, leading to electrode IV, resulted in an increase in the diameter of second semicircle, implying increased electron transfer resistance. According to the above explanation and previous reports [18,59], electron transfer resistance should be increased with the increase in GOD loading. However, the R_{et} value of electrode III was comparable to that of electrode I, even though the GOD loading was 1.6-times higher, whereas the

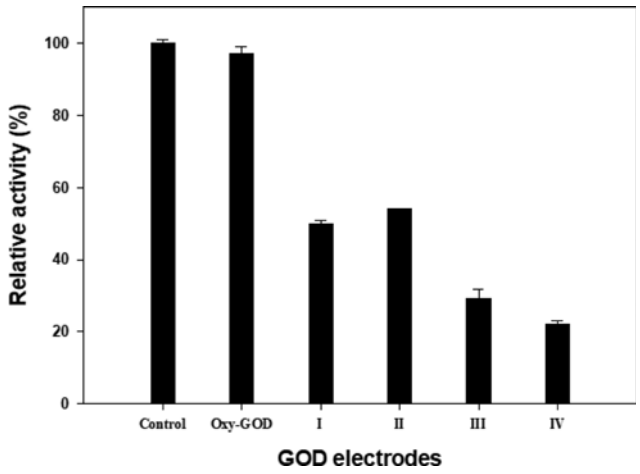

Fig. 8. Relative activities of free- and GOD-immobilized electrodes (I-IV). Control and oxy-GOD represent free GOD and $NaIO_4$-oxidized GOD, respectively.

resulting current by electrode III was much lower than that by electrode I. To explain this result, biochemical analysis of the immobilized GOD was performed in the next experiments.

4. Enzymatic Activities of GOD Immobilized on Electrodes

The relative activities of the four electrodes are shown in Fig. 8, which represent the ratio of specific activity of free and immobilized oxy-GOD to that of free native GOD (control). The relative activity of free oxy-GOD was 97±2%, indicating that the GOD activity was not reduced during the oxidation of the native GOD by $NaIO_4$. This result is in good accord with the previous report by Nakamura et al. [60], in which they demonstrated that carbohydrate on the peripheral surface of the GOD was oxidized to carbaldehyde with $NaIO_4$, and no significant alteration was brought about by this treatment in the catalytic parameters (K_m and k_{cat}), the immunological reactivity and the gross structure.

The relative activity of electrode I was 50±1%, which indicates that during the immobilization, the enzyme activity decreased twofold. The possible reduction in the activity of immobilized enzyme has been generally accepted, because of the internal and external mass transfer, and/or a shift in the optimal condition required for the substrate conversion [61]. Notably, however, the relative activities of electrode II were slightly greater than that of electrode I, which indicates that, while the AuNPs did not have any detrimental effect, they increased the catalytic activity of the enzyme. The enhancement of specific enzyme activity in the presence of AuNPs was demonstrated for lipases [62], α-amylase [63], and glucose oxidase [64,65], in which the AuNPs altered the catalytic properties of enzymes by increasing the affinity for enzyme-substrate formation, and enhancing their stability. The relative activity of electrode III was 1.7-times less than that of electrode I, while the relative activity of electrode IV was 2.3-times less than that of electrode II. The result clearly indicates that the specific activity of the double-layer GOD was lower than that of the single-layer GOD. According to Sakr et al. [66], the thicker the deposited enzyme layers, the more the layer limits the diffusion of the substrate to reach the enzyme, which results in a considerable decrease in the specific activity of the enzyme. The positive effect of AuNPs may be minimized at the highly diffusion-limited condition, due to the thick GOD layer. As mentioned (Table 1), the R_{et} value of the single- (electrode I) and double-layer GOD (electrode III) are comparable, but the current per GOD loading of electrode I was 2.2-times greater than that of electrode III. Together with electrochemical analysis, enzyme assay data clearly shows that the higher current generation by electrode I was mainly due to the higher activity of immobilized GOD on electrode I, than that on electrode III. The result shows that optimizing the configuration of GOD and AuNP layers can maximize current generation. The size of the AuNPs may also affect the performance of the electrodes. It has been generally known that smaller-sized AuNPs provide a higher surface area to volume ratio by allowing for more freedom in the orientation of the anchored enzyme, which leads to higher electrocatalytic activity [67,68]. In this study, 20 nm-diameter AuNPs were immobilized on the surface of electrode because AuNPs ranging 10-20 nm have previously shown a pronounced effect on the sensing signals of electrodes [16]. The performance of the enzyme electrode would be further enhanced if the particle sizes were optimized.

5. Application of the Optimally Configured ITO Electrodes for a High-power EFC

Since electrode II showed the best electrochemical performance, i.e., low electron transfer resistance and high enzymatic activity leading to high peak current, it was chosen as anode for EFC system. The BOD was chosen as cathode enzyme because of its stability in the presence of halide ions at neutral pH [69]. Preliminarily, the electrochemical performance of BOD electrode with or without AuNPs was evaluated by using CV in a PBS (pH 7.0) saturated with oxygen. Notably, 1.4-fold greater reduction peak current was obtained by introducing AuNPs (Fig. 9). The result indicates that AuNPs mediated electron transfer in the cathode in collaboration with PAA-PVI-Os-dCl-bpy, thereby enhancing the current gener-

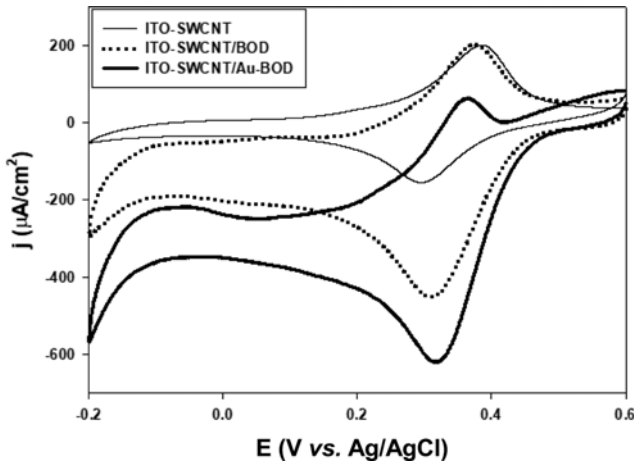

Fig. 9. Cyclic voltammograms of BOD-immobilized ITO electrodes with or without AuNPs; bare electrodes (thin solid line), ITO-SWCNT/BOD (dotted line) and ITO-SWCNT/Au-BOD (thick solid line). Electrodes were modified with redox mediator, PAA-PVI-Os-dCl-bpy and then cyclic voltammetry measurements were performed in PBS (pH 7.0) saturated with oxygen at scan rate of 10 mV/s.

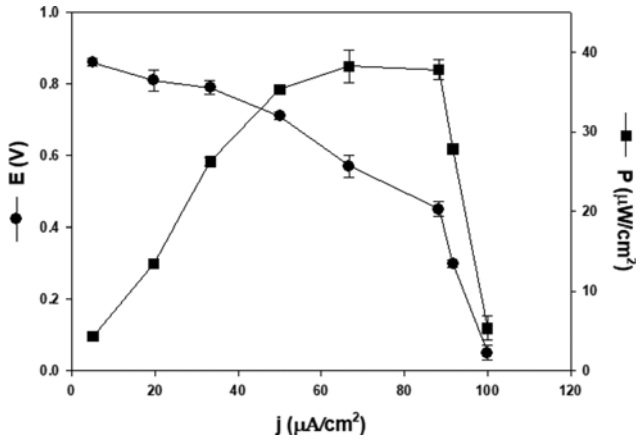

Fig. 10. The cell voltage (circle) and cell power (rectangular) curves under different discharge currents for EFCs consisting of electrode II (ITO-SWCNT-Au-GOD)/PVI-Os-dmo-bpy as anode and ITO-SWCNT/Au-BOD/PAA-PVI-Os-dCl-bpy as cathode. Measurements were performed in PBS (pH 7.0) supplemented with 30 mM of glucose with slow shaking. Electrolyte was saturated with oxygen before use.

ation. Enhanced catalytic response by AuNPs in BOD electrodes was also described in a previous report [70].

Accordingly, we tested the performance of an EFC, where the cathode was an electrode fabricated with AuNPs and BOD (ITO-SWCNT/Au-BOD), while still using electrode II as an anode. The PVI-Os-dmo-bpy and PAA-PVI-Os-dCl-bpy were used as anode- and cathode mediator, respectively. In glucose solution (30 mM), the EFC displayed an open circuit voltage (OCV) around 0.84 V, but cell voltage dropped off when current was drawn from cells (Fig. S4). Fig. 10 shows the discharge (polarization) profiles of the EFCs, measured for different discharge currents. The power density increased with increasing discharge current, reaching a maximum (38.2±2.0 $\mu W/cm^2$) at 0.57±0.03 V of a cell voltage under 66.7 $\mu A/cm^2$ of discharge current density. The power density of EFCs was still high at 88.3 $\mu A/cm^2$ of discharge current, but it dropped with further increase in discharge current. Fig. S5 shows the stability of EFCs. Cell voltage was maintained at 0.54 V under 66.7 $\mu A/cm^2$ of discharge current density for 48 h. We consider that the performance can be further improved if BOD enzyme and Os-polymer mediators are attached on the electrodes by covalent binding. Table S1 shows the power outputs of newly fabricated ITO-based EFCs using glucose as fuel [28,30]. Notably, the maximum power output obtained in this study was 27-fold greater than that of the other reported ITO-based EFCs.

The enhanced power generation achieved by our system was due to the optimal configuration of SWCNTs, AuNPs, and GOD layers on the surface of ITO electrodes as well as efficient electrical connection of enzyme redox centers to electrodes by Os-based redox mediators. The result clearly demonstrates successful development of high-power glucose EFCs using ITO-SWCNT-Au-GOD and ITO-SWCNT/Au-BOD as anode and cathode, respectively.

The poor electron transfer of ITO has been a barrier to the development of a high power EFC, even though it has the several advantages including a low background signal. The represented configuration of the nanomaterials allowed the development of the high power EFC system using ITO electrodes. To the best of our knowledge, the power density of the represented EFC fabricated with the optimally configured ITO electrodes was the highest among the previously reported ITO-based EFCs [23,38,71]. The proposed electrode fabrication method is promising for enhancing the stability of EFCs because CNT coating on the surface of ITO and covalent attachment of enzyme on electrodes make the enzyme electrode more stable than the mechanical compression of CNT-enzyme composite. The performance of EFCs will be further improved if EFC is equipped with systems for continuous supplying glucose and oxygen as well as improved cathode.

CONCLUSION

We achieved effective electron transfer on ITO electrodes functionalized with SWCNTs and AuNPs, with their subsequent conjugation of GOD affording anode electrodes that were suitable for the fabrication of high-power EFC. The large surface area-to-volume ratio and good conductivity of SWCNTs and AuNPs reduced the electron transfer resistance of ITO electrodes, and AuNPs improved the catalytic activity of GOD by increasing the affinity for enzyme-substrate formation while also enhancing its stability. We also found that single layer of AuNP-GOD on ITO modified with SWCNT afforded the best electrochemical performance, whereas the corresponding double layers increased electron transfer resistance, with decrease in specific catalytic activity resulting in lower peak currents. Power generation was enhanced by introducing AuNPs between BOD and SWCNTs on the cathode assembled in EFCs using the optimized GOD electrode as the anode. The novel technology used in this study for the adsorption of SWCNTs and covalent bindings of AuNPs-GOD on ITO could be also applied to improve the performance of transparent electrodes in biosensor. We believe the described characterization and application of SWCNT- and AuNP-modified ITO electrodes will facilitate the development of more practical ITO-based EFCs for implantable or patchable electrical devices.

ACKNOWLEDGEMENTS

This research was supported by the Basic Science Research Program through the National Research Foundation of Korea (NRF), funded by the Ministry of Education [2017R1D1A1B03029032].

SUPPORTING INFORMATION

Additional information as noted in the text. This information is available via the Internet at http://www.springer.com/chemistry/journal/11814.

RFERENCES

1. S. Cosnier, A. L. Goff and M. Holzinger, *Electrochem. Commun.*, **38**, 19 (2014).
2. Z. Zhong, Q. Li, T. Yang, W. Ge, Y. Lu, H. Chuantao and L. Aithua, *J. Electroanal. Chem.*, **823**, 723 (2018).

3. V. Scherbahn, M. T. Putze, B. Dietzel, T. Heinlein, J. J. Schneider and F. Lisdat, *Biosens. Bioelectron.*, **61**, 631 (2014).
4. V. Krikstolaityte, P. Lamberg, M. D. Toscano, M. Silow, O. Eicher-Lorka, A. Ramanavicius, G. Niaura, L. Abariute, T. Ruzgas and S. Shleev, *Fuel Cells*, **14**, 792 (2014).
5. M. Zayats, B. Willner and I. Willner, *Electroanal.*, **20**, 583 (2008).
6. A. Zebda, C. Gondran, A. L. Goff, M. Holzinger, P. Cinquin and S. Cosnier, *Nat. Commun.*, **2**, 370 (2011).
7. M. Falk, Z. Blum and S. Shleev, *Electrochim. Acta.*, **82**, 191 (2012).
8. M. Zhao, Y. Gao, J. Sun and F. Gao, *Anal. Chem.*, **87**, 2615 (2015).
9. O. Yehezkeli, R. Tel-Vered, S. Raichlin and I. Willner, *ACS Nano*, **5**, 2385 (2011).
10. A. Zebda, S. Cosnier, J.-P. Alcaraz, M. Holzinger, A. LeGoff, C. Gondron, F. Boucher, F. Giroud, K. Gorgy, H. Lamraoui and P. Cinquin, *Sci. Rep.*, **3**, 1516 (2013).
11. E. H. Yu and K. Scott, *Energies*, **3**, 23 (2010).
12. A. Heller, *Curr. Opin. Chem. Biol.*, **10**, 664 (2006).
13. N. Mano, F. Mao and A. Heller, *ChemBioChem.*, **5**, 1703 (2004).
14. C. H. Kwon, S.-H. Lee, Y.-B. Choi, J. A. Lee, S. H. Kim, H.-H. Kim, G. M. Spinks, G. G. Wallace, M. D. Lima, M. E. Kozlov, R. H. Baughman and S. J. Kim, *Nat. Commun.*, **5**, 3928 (2014).
15. M. Christwardana, K. J. Kim and Y. Kwon, *Sci. Rep.*, **6**, 30128 (2016).
16. W. Yang, J. Wang, S. Zhao, Y. Sun and C. Sun, *Electrochem. Commun.*, **8**, 665 (2006).
17. J. Zhang, M. Feng and H. Tachikawa, *Biosens. Bioelectron.*, **22**, 3036 (2007).
18. X. Wang, S. B. Kim, D. Khang, H.-H. Kim and C.-J. Kim, *Biochem. Eng. J.*, **112**, 20 (2016).
19. L. Fu and A. M. Yu, *Rev. Adv. Mater. Sci.*, **36**, 40 (2014).
20. M. A. Aziz and H. Yang, *Bull. Korean Chem. Soc.*, **28**, 1171 (2007).
21. C. K. Choi, C. H. Margraves, S. I. Jun, A. E. English, P. D. Rack and K. D. Kihm, *Sensors*, **8**, 3257 (2008).
22. D. M. Kalaskar, S. Demoustier-Champagne and C. C. Dupont-Gillain, *Colloids Surfs. B Biointerfaces*, **111**, 134 (2013).
23. M. A. Aziz, S. Park, S. Jon and H. Yang, *Chem. Commun.*, 2610 (2007).
24. L. A. Geddes and R. Roeder, *Ann. Biomed. Eng.*, **31**, 879 (2003).
25. C. Exley, *Environ. Sci.: Process Impacts*, **15**, 1807 (2013).
26. R. Peters and J. M. Walshe, *Proc. R. Soc. London B: Biol. Sci.*, **166**, 273 (1966).
27. S.-W. Yeung, T. M.-H. Lee, H. Cai and I.-M. Hsing, *Nucl. Acids Res.*, **34**, e118 (2006).
28. E. Gonzalez.-Arribas, T. Bobrowski, C. D. Bari, K. Sliozberg, R. Ludwig, M. D. Toscano, A. L. D. Lacey, M. Pita, W. Schuhmann and S. Shleev, *Biosens. Bioelectron.*, **97**, 46 (2017).
29. Y. Ayato and W. Sugimoto, *ECS Transact.*, **66**, 29 (2015).
30. T. Bobrowski, E. G. Arribas, R. Ludwig, M. D. Toscano, S. Shleev and W. Schuhmann, *Biosens. Bioelectron.*, **101**, 84 (2018).
31. S. Pichardo, D. Gutierrez-Praena, M. Puerto, E. Sanchez, A. Grilo, A. M. Camean and A. Jos, *Toxycol. in Vitro*, **26**, 672 (2012).
32. A. Jos, S. Pichardo, M. Puerto, E. Sanchez, A. Grilo and A. M. Camean, *Toxycol. in Vitro*, **23**, 1419 (2009).
33. B. A. Gregg, and A. Heller, *J. Phys. Chem.*, **95**, 5970 (1991).
34. H.-H. Kim, N. Mano, Y. Zhang and A. Heller, *J. Electrochem. Soc.*, **150**, A209 (2003).
35. S. Timur, B. Haghighi, Jan Tkac, Nurdan Pazarhoglu, A. Telefoncu and L. Gorton, *Bioelectrochem.*, **71**, 38 (2007).
36. G. Kenausis, C. Taylor, I. Katakis and A. Heller, *J. Chem. Soc. Faraday Trans.*, **92**, 4131 (1996).
37. W.-Y. Jeon, Y.-B. Choi and H.-H. Kim, *Sensors*, **15**, 31083 (2015).
38. M. A. Aziz, K. Jo, J.-A. Lee, M. R. H. Akanda, D. Sung, S. Jon and H. Yang, *Electroanal.*, **22**, 2615 (2010).
39. S. Attal, R. Thiruvengadathan and O. Regev, *Anal. Chem.*, **78**, 8098 (2006).
40. H. Wen, V. Nallathambi, D. Chakraborty and S. C. Barton, *Microchim Acta.*, **175**, 283 (2011).
41. J. I. Paredes and M. Burghard, *Langmuir*, **20**, 5149 (2004).
42. M. S. Dresselhaus, G. Dresselhaus, R. Saito and A. Jorio, *Phys. Rep.*, **409**, 47 (2005).
43. J. Lin, C. He, Y. Zhao and S. Zhang, *Actuators B*, **137**, 768 (2009).
44. C. Dhand, S. K. Arya, S. P. Singh, B. P. Singh, M. Datta and B. D. Malhotra, *Carbon*, **46**, 1727 (2008).
45. K. Sone and M. Yagi, *Electroanalysis*, **21**, 144 (2009).
46. H. Cao, Y. Zhu, L. Tang, X. Yang and C. Li, *Electroanalysis*, **20**, 2223 (2008).
47. V. Ganesh, D. L. Maheswari and S. Berchmans, *Electrochim. Acta*, **56**, 1197 (2011).
48. H.-Z. Zhao, J.-J. Sun, J. Song and Q.-Z. Yang, *Carbon*, **48**, 1508 (2010).
49. K. A. Wepasnick, B. A. Smith, J. L. Bitter and D. H. Fairbrother, *Anal. Bioanal. Chem.*, **396**, 1003 (2010).
50. Q. Shi, D. Yang, Y. Su, J. Li, Z. Jiang, Y. Jiang and W. Yuan, *J. Nanopart. Res.*, **9**, 1205 (2007).
51. D. Ivnitski, K. artyushkova, R. A. Rincon, P. Atanassov, H. R. Luckarift and G. R. Johnson, *Small*, **4**, 357 (2008).
52. M. L. Verma, M. Naebe, C. J. Barrow and M. Puri, *Plos One*, **8**, e73642 (2013).
53. G. Hernandez-Cancel, D. Suazo-Davila, A. J. Ojeda-Cruzado, D. Garcia-Torres, C. R. Cabrera and K. Griebenow, *J. Nanotechnol.*, **13**, 70 (2015).
54. Y. Joseph, I. Besnard, M. Rosenberger, B. Guse, H.-G. Nothofer, J. M. Wessels, U. Wild, A. Knop-Gericke, D. Su, R. Schlogl, A. Yasuda and T. Vossmeyer, *J. Phys. Chem. B*, **107**, 7406 (2003).
55. H. Fayazfar, A. Afshar, M. Dolati and A. Dolati, *Anal. Chim. Acta.*, **836**, 34 (2014).
56. X. Li, X. Zhao, M.-S. Wang, K.-J. Zhang, Y. Huang, M.-Z. Qu, Z.-L. Yu, D.-S. Geng, W.-G. Zhao and J.-M. Zheng, *RSC Adv.*, **7**, 24359 (2017).
57. A. T. Ezhilvilian, V. Veeramani, S.-M. Chen, R. Madhu, C. H. Kwak, Y. S. Huh and Y.-K. Han, *Sci. Rep.*, **5**, 18390 (2015).
58. X. Chen, X. Yan, K. A. Khor and B. K. Tay, *Biosens. Bioelectron.*, **22**, 3256 (2007).
59. H. Zhao and H. Ju, *Anal. Biochem.*, **350**, 138 (2006).
60. S. Nakamura, S. Hayashi and K. Koga, *Biochim. Biophys. Acta.*, **445**, 294 (1976).
61. S. Mutlu, M. Mutlu and E. Piskin, *Biochem. Eng. J.*, **1**, 39 (1998).
62. C.-S. Wu, C.-T. Wu, Y.-S. Yang and F.-H. Ko, *Chem. Commun.*, 5327 (2008).
63. J. Deka, A. Paul and A. Chattopadhyay, *RSC Adv.*, **2**, 4736 (2012).
64. H. Papa, M. Gaillard, L. Gonzalez and J. Chatterjee, *Biosensors*, **4**, 449 (2014).
65. S. Thibault, H. Aubriet and C. Arnoult, *Microchim. Acta*, **163**, 211

(2008).
66. O. S. Sakr and G. Borchard, *Biomolecules*, **14**, 2117 (2013).
67. A. de la Escosura-Muniz, C. Parolo, F. Marian and A. Mekoci, *Nanoscale*, **3**, 3350 (2011).
68. H. Zhang, H. Lu and N. Hu, *J. Phys. Chem. B*, **110**, 2171 (2006).
69. F. Tasca, D. Farias, C. Castro, C. Acuna-Rougier and R. Antiochia, *Plos One*, **10**, e0132181 (2015).
70. P. Kannan, H. Chen, V. T. Lee and D. H. Kim, *Talanta*, **86**, 400 (2011).
71. Y. Wu, X. Feng, S. Zhou, H. Shi, H. Wu, S. Zhao and W. Song, *Microchim. Acta*, **180**, 1325 (2013).

Supporting Information

Fabrication of optimally configured layers of SWCNTs, gold nanoparticles, and glucose oxidase on ITO electrodes for high-power enzymatic biofuel cells

Xue Wang*, Joong Hyun Kim, Yong Bong Choi***, Hyug-Han Kim***, and Chang-Joon Kim*,†**

*Department of Chemical Engineering and RIGET, Gyeongsang National University, 501 Jinju-daero, Jinju, Gyeongnam 52828, Korea
**Medical Device Development Center, Daegu Gyeongbuk Medical Innovation Foundation, Daegue 41061, Korea
***Department of Chemistry, Dankook University, Cheonan 31116, Korea
(*Received 26 December 2018 • accepted 20 April 2019*)

Instrumental Analysis of GOD-immobilized ITO Electrodes

The distribution of SWCNTs in the deposited layer and its thickness were analyzed by high-resolution Raman microscopy (LabRAM, HR Evolution, HORIBA, France). SWCNTs immobilized on ITO slides (1 cm×1 cm) were irradiated by 633-nm laser through an Olympus 50× objective, and Raman-scattered radiation was collected by the same objective (integration time=8 s), and dispersed using a 600 groove/mm grating. Images were acquired over a 50 μm×50 μm area, and Raman spectra were recorded with a step size of 2.5 μm, and are shown in Fig. S1.

JEOL JSM-7610F microscopy with racer northern EDX system (JEOL Ltd., Japan) was used for the elemental analysis of the fabricated four electrodes at the accelerating voltage of 20 kV. Samples were placed on the sample holders supported by 1-min sputter coating of Pt, and the spectra are shown in Fig. S2.

Operational Stability of EFCs

The operational stability of the developed EFC was evaluated by measuring cell voltage versus time under 66.7 μA/cm^2 of discharge current. Measurement was performed in PBS (pH 7.0) supplemented with 30 mM of glucose with slow shaking. Electrolyte was replaced every 12 h and saturated with oxygen before use. The result was shown in Fig. S5.

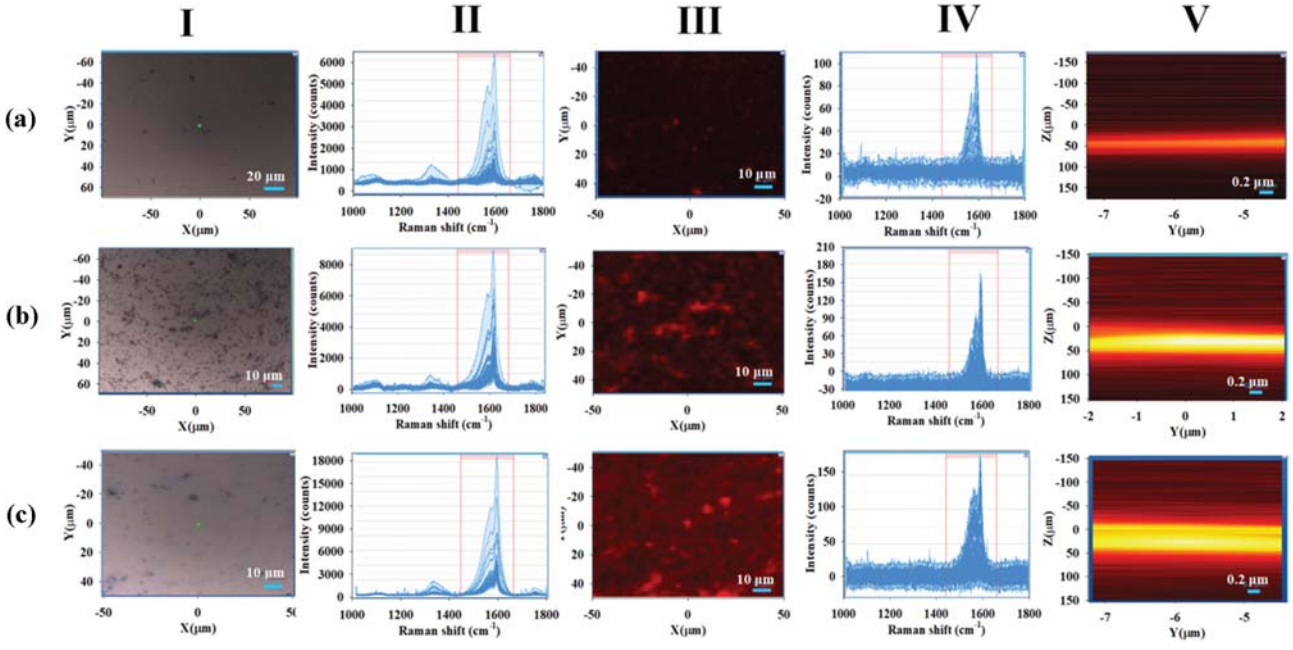

Fig. S1. SWCNT distribution on the surface of ITO electrodes depending on the loading amount of SWCNTs ((a) 9; (b) 18; (c) 37) μg/cm^2). The Roman numbers represent (I) bright field microscopy images, (II) collected Raman scattering over the X and Y axes of the samples, (III) images of Raman mappings using the collected Raman scatterings II, (IV) collected Raman scatterings over the Z and Y axes of the samples, and (V) images of Raman mappings using the collected Raman scatterings IV.

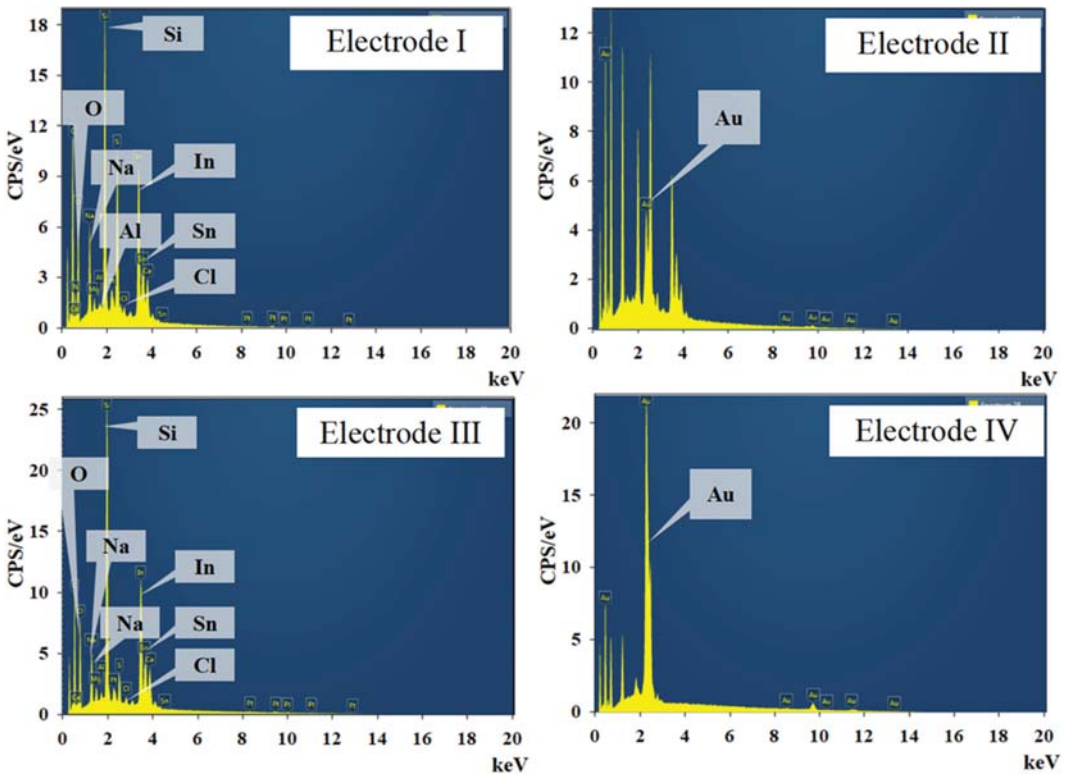

Fig. S2. EDX spectra of electrodes I, II, III, and IV.

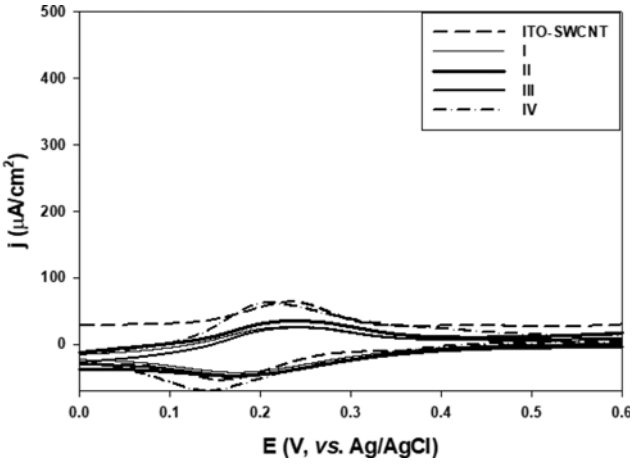

Fig. S3. Cyclic voltammograms of electrode I (ITO-SWCNT-GOD), II (ITO-SWCNT-Au-GOD), III (ITO-SWCNT-GOD-GOD) and IV (ITO-SWCNT-Au-GOD-Au-GOD) in the absence of glucose in PBS (pH 7.0) at scan rate of 10 mV/s. Electrodes were modified with redox polymer (PVI-Os-dme-bpy).

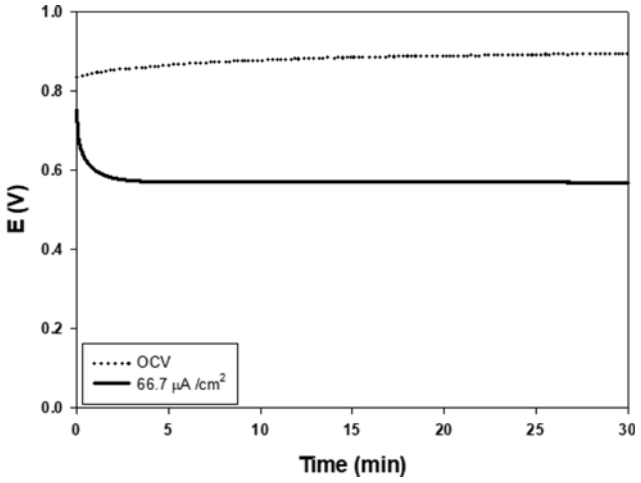

Fig. S4. The cell voltage curve under discharge current (66.7 μA/cm^2) for EFC consisting of electrode II (ITO-SWCNT-Au-GOD)/PVI-Os-dmo-bpy as anode and ITO-SWCNT/Au-BOD/PAA-PVI-Os-dCl-bpy as cathode. Measurements were performed in PBS (pH 7.0) supplemented with 30 mM of glucose. Electrolyte was saturated with oxygen before use.

Table S1. Comparison of the construction and power out of recent ITO-based EFCs utilizing glucose as fuel

Nanostruture	*Enzymes (anode/cathode)	Mediator	Power output ($\mu W/cm^2$)	References
Indium tin oxide nanoparticle	CDH/ BOD	Mediator-free	1.4	28
Indium tin oxide nanoparticle	GDH/BOD	Mediator-free	0.09	30
SWCNT and gold nanoparticles	GOD/BOD	Os polymer	38	This work

*GDH, CDH, GOD, and BOD represent glucose dehydrogenase, cellobiose dehydrogenase, glucose oxidase, and bilirubin oxidase

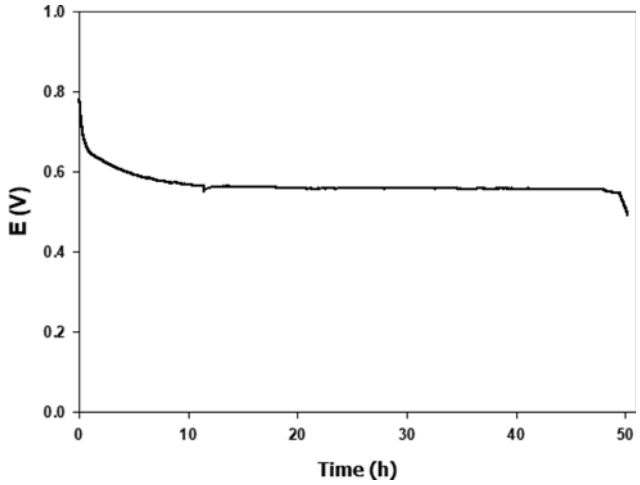

Fig. S5. Operational stability under discharge current (66.7 $\mu A/cm^2$) for EFC consisting of electrode II (ITO-SWCNT-Au-GOD)/ PVI-Os-dmo-bpy as anode, and ITO-SWCNT/Au-BOD/ PAA-PVI-Os-dCl-bpy as cathode. Measurements were performed in PBS (pH 7.0) supplemented with 30 mM of glucose with slow shaking. Electrolyte was replaced every 12 and saturated with oxygen before use.